 Related Commentary, page 657

Chikungunya disease in nonhuman primates involves long-term viral persistence in macrophages

Karine Labadie,[1,2] Thibaut Larcher,[3] Christophe Joubert,[1,2] Abdelkrim Mannioui,[1,2] Benoit Delache,[1,2] Patricia Brochard,[1,2] Lydie Guigand,[3] Laurence Dubreil,[3] Pierre Lebon,[4] Bernard Verrier,[5] Xavier de Lamballerie,[6,7] Andreas Suhrbier,[8] Yan Cherel,[3] Roger Le Grand,[1,2] and Pierre Roques[1,2]

[1]CEA, Division of Immuno-Virology/Institute of Emerging Diseases and Innovative Therapies (iMETI), Fontenay-aux-Roses, France. [2]UMR-E1, Paris-Sud 11, Orsay, France. [3]INRA, UMR 703, Ecole Nationale Vétérinaire, Nantes, France. [4]Université Paris V, Hôpital Cochin-St Vincent de Paul, Service de virologie, Paris, France. [5]CNRS, UMR 5086, IBCP-IFR 128, Lyon, France. [6]Université de la Méditerranée, Unité des Virus Emergents, Marseille, France. [7]Institut de Recherche pour le Développement, Marseille, France. [8]Australian Centre for International and Tropical Health, Queensland Institute of Medical Research, Brisbane, Australia.

Chikungunya virus (CHIKV) is a mosquito-borne alphavirus that induces in humans a disease characterized by fever, rash, and pain in muscles and joints. The recent emergence or reemergence of CHIKV in the Indian Ocean Islands and India has stressed the need to better understand the pathogenesis of this disease. Previous CHIKV disease models have used young or immunodeficient mice, but these do not recapitulate human disease patterns and are unsuitable for testing immune-based therapies. Herein, we describe what we believe to be a new model for CHIKV infection in adult, immunocompetent cynomolgus macaques. CHIKV infection in these animals recapitulated the viral, clinical, and pathological features observed in human disease. In the macaques, long-term CHIKV infection was observed in joints, muscles, lymphoid organs, and liver, which could explain the long-lasting CHIKV disease symptoms observed in humans. In addition, the study identified macrophages as the main cellular reservoirs during the late stages of CHIKV infection in vivo. This model of CHIKV physiopathology should allow the development of new therapeutic and/or prophylactic strategies.

Introduction

Chikungunya virus (CHIKV) is a mosquito-borne alphavirus (family *Togaviridae*) first described in Africa in 1953 (1). CHIKV belongs to a group of widely distributed arthrogenic alphaviruses, which include the Australian Ross River virus (RRV), the African O'nyong nyong virus, and the Mayaro virus. CHIKV disease is characterized by high fever, arthralgia/arthritis, papular or maculopapular skin rash, myalgia, and headache. Recovery generally occurred within a few weeks, although persistent CHIKV-induced arthralgia has been reported in 12% of patients (2–4). No specific antiviral therapy is currently available, and treatment generally involves analgesics, antipyretics, and/or nonsteroidal antiinflammatory drugs.

Several outbreaks of CHIKV disease have been reported in Africa and Asia over the last 50 years (5–9). During 2004–2007, the largest documented outbreak of CHIKV disease occurred in the Indian Ocean Islands and India. Particularly affected was Reunion Island, an overseas department of France with a Western health care system. During 2005 and 2006, about 300,000 cases of CHIKV disease (38% of the population) were reported on Reunion Island (10, 11). Of these, approximately 2,200 patients (0.8%) required hospitalization, and more than 250 deaths (0.1%) were reported. Mortality was generally restricted to elderly patients and patients with significant comorbidities. The Reunion Island epidemic was characterized not only by the most common CHIKV symptoms (fever, 95.3%; incapacitating polyarthralgia, 95.2%; headache, 75.8%; myalgia, 64.5%; and cutaneous manifestations, 34.9%; ref. 12), but also by a variety of atypical clinical symptoms, such as gastrointestinal disorders (diarrhea, vomiting, or hepatitis, 21%), neurological complications (encephalitis or meningoencephalitis, 12%), and heart disease (myocarditis or pericarditis, 5%) (13). These atypical cases were mostly observed in young children, the elderly, and patients with comorbidities (14). A few cases of maternoneonatal viral transmission were also reported (about 3 per 1,000 births). In addition, the Reunion Island outbreak appeared to involve more severe and persistent rheumatic disease, with several studies showing that 50%–75% of CHIKV-infected adults had joint pain 1 year after infection (15–17). CHIKV has been declared a high-priority pathogen by the NIH.

To date, little is known about the pathophysiological mechanisms of CHIKV infection in humans, and the only available CHIKV disease models involve infection of very young mice or mice defective in type 1 IFN signaling (18, 19). These models do not recapitulate the disease pattern seen in humans and are unsuitable for testing immunological interventions. Nonhuman primates are particularly relevant for studies of pathogenesis and assessment of therapies because their physiology and immune system are similar to those in humans (20–23). Nonhuman primates are susceptible to CHIKV infection and probably act as part of the natural reservoir in Africa and Asia (24–30). However, previous studies of CHIKV infection in nonhuman primates have not focused on analyzing viral pathogenesis (24, 31, 32). To our knowledge, CHIKV cell and tissue tropism in humans has also not been extensively studied to date. CHIKV antigens have been detected by immunohistochemistry in muscle satellite cells of muscle biopsies from 2 patients with a myositic syndrome (33) and in fibroblasts of the joint capsule, skeletal muscle, and dermis from a fatal neonatal case (18). In vitro studies have shown that other cell types, such as

Conflict of interest: The authors have declared that no conflict of interest exists.
Citation for this article: *J Clin Invest.* 2010;120(3):894–906. doi:10.1172/JCI40104.

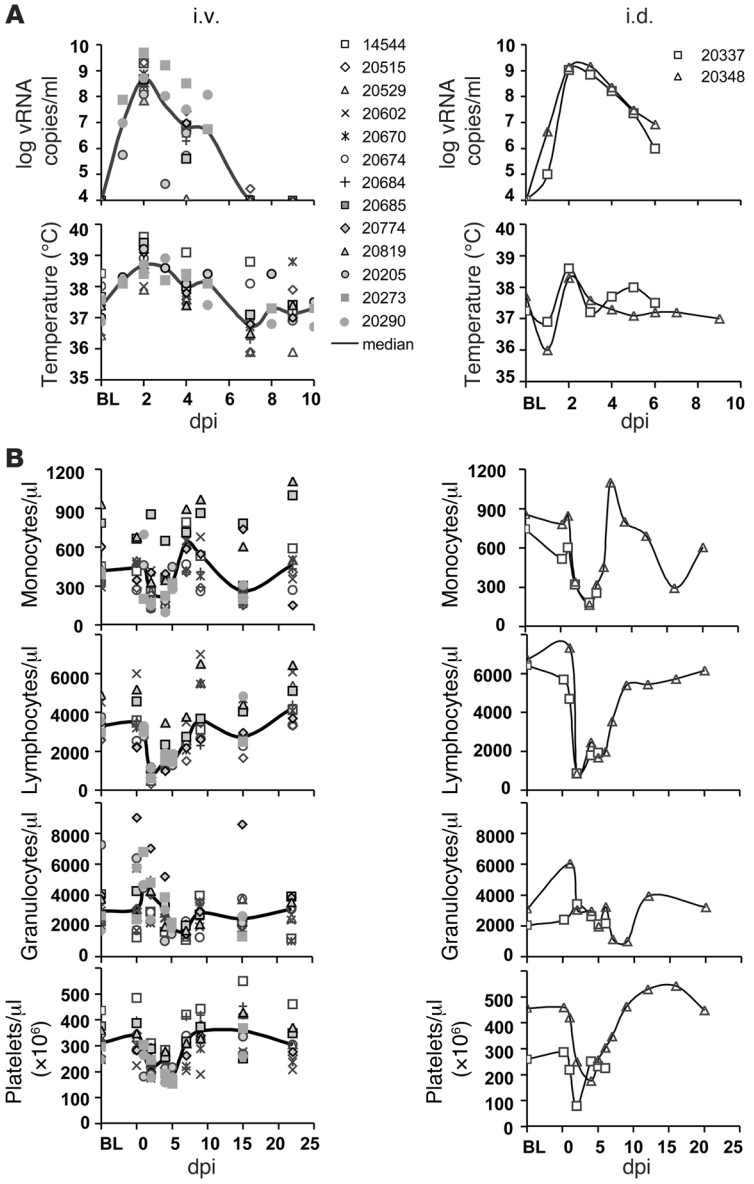

Figure 1
CHIKV infection in adult cynomolgus macaques. (**A**) Kinetics of viral replication and rectal temperatures of 15 animals following i.v. ($n = 13$) or i.d. ($n = 2$) inoculation of 10^3 PFU CHIKV strain LR2006-OPY1. Viral load was evaluated by quantitative RT-PCR. BL, baseline. (**B**) Kinetics of blood cell counts in animals following i.v. or i.d. inoculation of 10^3 PFU CHIKV.

human epithelial and endothelial cells, primary fibroblasts, and, to a lesser extent, monocyte-derived macrophages, are also able to sustain productive CHIKV infections (34).

Herein, we describe the characteristics of CHIKV infection in cynomolgus macaques (*Macaca fascicularis*) using a CHIKV isolate from a patient infected during the recent Reunion Island epidemic (35); the infection produced viremia and clinical signs similar to those seen in humans. Using this model, we investigated viral replication sites and tissue reservoirs during the early and later stages of infection. We showed that CHIKV targeted lymphoid tissues, liver, central nervous system, joint, and muscle during the acute phase of infection and mainly infected macrophages, dendritic cells, and some endothelial cells. At later stages of infection, CHIKV persisted in lymphoid organs, liver, joint, and muscle and was found in macrophages up to 3 months after viral inoculation. Our results thus identify macrophages as the main cellular reservoir of persistent CHIKV infection, potentially explaining long-lasting symptoms observed in humans. These insights into CHIKV pathogenesis should facilitate future development of more effective treatments for CHIKV disease.

Results

CHIKV infection in cynomolgus macaques mimics CHIKV infection in humans. Herein we describe a nonhuman primate model of infection with the CHIKV isolate LR2006-OPY1, obtained from a patient infected during the recent Reunion Island epidemic (35). This model allowed for analysis of CHIKV tropism and examination of the pathophysiological basis of CHIKV disease. We inoculated 13 adult cynomolgus macaques (*Macaca fascicularis*, 3–5 years old) i.v. with 10^3 PFU CHIKV, corresponding to 10^5 viral RNA (vRNA) copies. This amount of vRNA is similar to the amount of virus secreted from salivary glands of mosquitoes collected from Reunion Island and artificially infected with CHIKV strains isolated from the Reunion outbreak (36). In parallel, 2 cynomolgus macaques, animals 20337 and 20348, were inoculated intradermally (i.d.) with 10^3 PFU to compare the effects of this inoculation route on clinical and biological parameters. Virus was detected by real-time RT-PCR in the plasma of infected animals from day 1 after i.v. or i.d. CHIKV inoculation. Viremia in both i.v.- and i.d.-inoculated animals reached a peak by 2 days postinoculation (dpi), with viral loads ranging from 7×10^7 to 5×10^9 vRNA copies/ml and viremia persisting until 6 or 7 dpi (Figure 1A). Although CHIK viremia has not been extensively studied in humans, studies to date suggest a short duration (not exceeding 1 week in most patients), with viral loads ranging from 1×10^3 to 1.2×10^{10} vRNA copies/ml (37–39). These prior findings in humans are consistent with the data described herein for macaques.

Clinically, monkeys developed a high fever by day 1 or 2 (up to 39.6°C), regardless of the inoculation route (Figure 1A). A similar level of fever was observed in humans during the Reunion Island outbreak (40). The fever in the monkeys remained significantly above baseline from 2 dpi ($P = 0.0015$, Mann Whitney U test [MWU]) until 7 dpi ($P < 0.02$, MWU). In the first week after inoculation, all animals developed morbilliform skin rashes of varying intensities. These cutaneous manifestations were similar to those observed in infected patients (17, 41). Gingival bleeding was also observed in half the infected animals. Gingivorrhagia has been previously reported in humans, mainly in CHIKV-infected children (2, 41). Other substantial manifestations observed during the CHIKV Reunion Island epidemic, such as arthralgia, headache, or myalgia, were difficult to evaluate in an animal model.

Serum of 5 animals was tested for aspartate transaminase (AST) and alanine transaminase (ALT) levels. All tested animals exhibited elevated levels of AST (2.5 times higher at 4 dpi; $P < 0.05$, Wilcoxon rank test) and ALT (1.8 times higher at 10 dpi; $P < 0.05$, Wilcoxon

Table 1
Virological and clinical outcomes were dependent on inoculation dose

n	Dose (PFU)	Peak viremia Day	Peak viremia vRNA copies/ml	Clinical signs
3	10^8	1	$>10^{10}$	Meningoencephalitis, death
1	10^8	<2	5×10^9	Fever, rash, subcutaneous edema, joint effusion
1	10^7	1	5×10^9	Fever, rash, joint effusion
1	10^6	2	10^9	Fever, rash
1	10^5	2	5×10^8	Fever, rash
3	10^3	2–3	5×10^8	Fever, with or without rash
1	10^2	3	10^8	Fever, rash
1	10^1	4	10^8	None
1	10^1	No	Negative	None

rank test; Supplemental Figure 1; supplemental material available online with this article; doi:10.1172/JCI40104DS1). AST and ALT levels remained significantly elevated even at 15 dpi ($P < 0.05$, Wilcoxon rank test). This pattern of biochemical changes is consistent with data from CHIKV patients recently described by Ng and colleagues (42) and is indicative of liver or muscle injury.

All i.v.- or i.d.-infected animals showed substantial and significant monocytopenia, lymphopenia, granulocytosis, and thrombocytopenia compared with uninfected animals ($P = 0.012$, 0.012, 0.028, and 0.03, respectively, MWU; Figure 1B and Supplemental Table 1). These changes were associated with peak viremia, with the nadir occurring between 2 and 4 dpi, and returned to normal by 10–15 dpi. Little information about hematopoietic cell numbers is available for human cases, although leukopenia is often observed during CHIKV infection (4, 17, 42).

To study the effect of the inoculation dose, 13 additional monkeys were inoculated with various doses of CHIKV, ranging from 10^1 to 10^8 PFU (Table 1). A clear relationship emerged between the inoculation dose and the period and magnitude of the viremia. The AUC of viremia over 0–10 dpi significantly correlated with the inoculation dose ($r^2 = 0.71$, $P < 0.024$; data not shown). Monkeys could be classified into 3 groups according to the inoculation dose and clinical signs: (a) in animals inoculated with a low dose of CHIKV (10^1 PFU), viral replication was detected in plasma of 50% of the animals and no clinical signs were observed; (b) in animals inoculated with an intermediate dose (10^2–10^6 PFU), viremia was associated with fever and rash; (c) in animals inoculated with a high dose (≥10^7 PFU), swelling in wrist and ankle joints, clinical signs of meningoencephalitis (hunching and wobbling, as well as

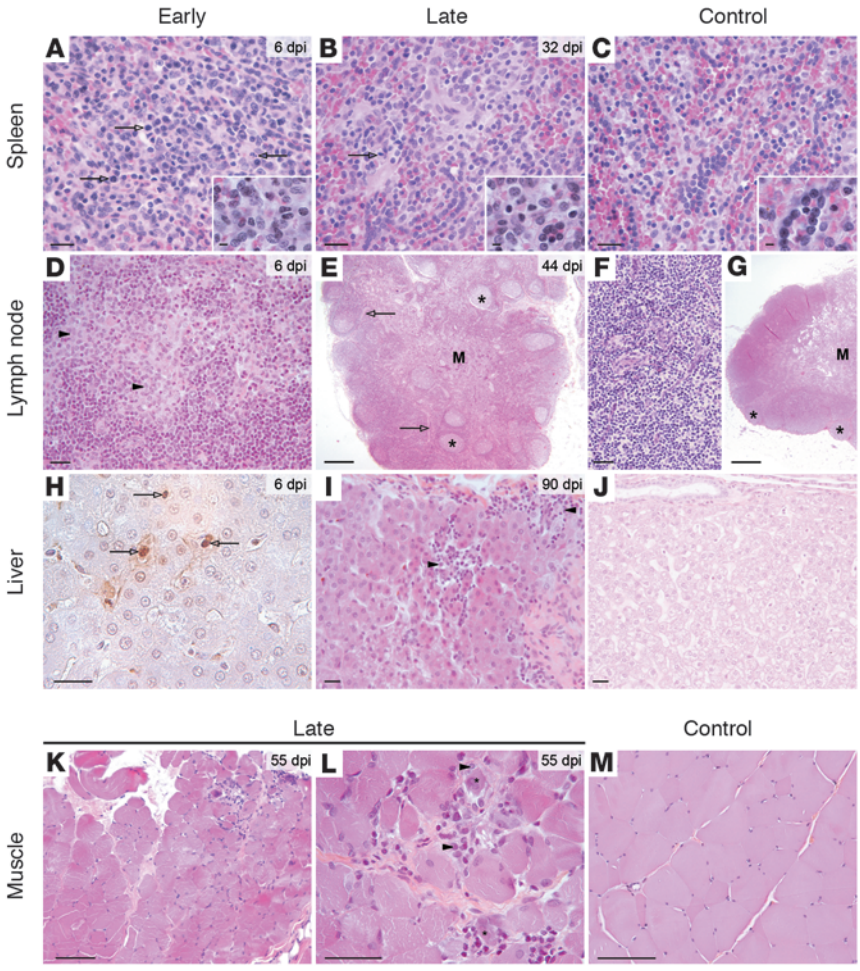

Figure 2
Lesions observed in tissues collected from 12 macaques inoculated with intermediate doses of CHIKV. Histology of tissues from CHIKV-infected macaques. (**A**) Spleen, 6 dpi. Density of mononuclear cells was diffusely increased in the red pulp. These mononuclear cells corresponded mostly to macrophages with abundant cytoplasm and large nucleolated nucleus (inset). Some mononuclear cells were undergoing mitosis (arrows). (**B**) Spleen, 32 dpi. Macrophages were still numerous in the red pulp; a few mitotic cells were visible (arrow). (**C**) Normal spleen. Red pulp contained numerous red blood cells. (**D**) Lymph node, 6 dpi. The cortex was distended by numerous macrophages (some denoted by arrowheads). (**E**) Lymph node, 44 dpi. Severe follicular enlargement (asterisks) was associated with macrophage infiltration. Postcapillary venules of the T-dependent area (arrows) and medulla (M) are indicated. (**F** and **G**) Normal lymph node. Lymphoid follicles (asterisks) and medulla are indicated. (**H**) Liver, 6 dpi. The number of apoptotic hepatocytes with nuclei (arrows), detected by TUNEL assay, increased. (**I**) Liver, 90 dpi. Multifocal interstitial mononuclear cell infiltration (arrowheads) was observed in the liver parenchyma. (**J**) Normal liver. (**K** and **L**) Skeletal muscle, 55 dpi. Mild multifocal necrosis of muscle fibers (asterisk) was associated with infiltration by mononuclear cells, including macrophages (arrowheads). (**M**) Normal muscle. (**A**–**G** and **I**–**M**) Hematoxylin eosin safran stain. (**H**) In situ detection of cell death using TUNEL staining. Scale bars: 100 μm (**A**–**D**, **F**, and **H**–**M**); 10 μm (insets); 1 mm (**E** and **G**).

Table 2
Histological lesions observed in intermediate dose–inoculated macaques

Lesion	dpi						
	6	19	32	44	55	90	97
Spleen and lymph nodes							
Histiocytosis	1	2	2	1	2	2	1
T cell area hypertrophy	1	2	2	0	0	0	0
Follicular enlargement	0	0	2	1	1	2	2
Liver							
Hemosiderosis	0	2	2	0	2	2	2
Hydropic degeneration	1	0	0	0	1	0	0
Interstitial hepatitis	0	0	0	1	2	2	1
Striated muscles							
Focal necrosis	0	0	0	0	1	0	0

Values denote total number of lesions. $n = 2$ for all time points, except 6 and 44 dpi ($n = 1$).

asthenia and ataxia), and/or mortality were observed. In the high-dose group, levels of monocytopenia, lymphopenia, and granulocytosis were not statistically different from those of the other infected animals ($P = 0.3$, 0.43, and 0.43, respectively, MWU; Supplemental Table 1). The neurological complications and fatalities were similar to the severe forms of disease described in humans during the Reunion Island outbreak (13, 43). The present study focused on the animals receiving intermediate- or high-dose CHIKV inoculations.

The clinical and biological parameters seen in this macaque model were remarkably similar to those reported in patients infected during the Reunion Island epidemic. Importantly, the magnitude and virulence of infection was dependent on the inoculation dose, with larger inocula resulting in earlier and higher peak viremias and greater severity of clinical symptoms (Table 1). Finally, the inoculation route did not influence CHIKV infection or disease in macaques inoculated with the intermediate 10^3-PFU dose.

Infected macaque tissues display extensive mononuclear cell infiltration. Various tissues, collected at 6, 19, 32, 44, 55, 90, and 97 dpi from 12 animals inoculated with intermediate doses of CHIKV, were examined by histology and compared with tissues from control uninfected animals (Figure 2 and Table 2). Major abnormalities were observed in spleen and lymph nodes of all animals from 6 dpi. Severe and persistent histiocytosis was observed in the spleen, appearing as an infiltrate in the red pulp consisting of mononuclear cells, with abundant eosinophilic cytoplasm, euchromatic nucleus, and prominent nucleolus, characteristic of macrophages (Figure 2, A and B, and Supplemental Figure 2). Lymph nodes also showed extensive infiltration of mononuclear cells, which were found mainly in the cortex and, to a lesser extent, in the medulla (Figure 2D). Severe follicular enlargement was associated with mononuclear cell infiltration at 32–44 dpi (Figure 2E). This decreased in severity thereafter, but was still present with mild intensity on 97 dpi.

In liver, we observed mild to marked centrolobular hepatocytic hydropic degeneration. TUNEL assays revealed abnormally high levels of hepatocyte death, mainly through apoptosis, peaking at 6 dpi (Figure 2H), and this was associated with the increased serum AST and ALT levels described above (Supplemental Figure 1). This early apoptotic process might result in part from hyperthermia (Figure 1A), as described previously in pigs and dogs (44). Between 44 and 90 dpi, all tested animals exhibited mild multifocal interstitial mononuclear cell infiltration of the hepatic parenchyma (Figure 2I). In the liver, between 6 and 97 dpi, large amounts of intracytoplasmic granular pigment (stained blue using Perls stain for hemosiderin) was observed in Kupffer cells. Similar hemosiderin deposition in Kupffer cells has been previously observed in other viral infections (45, 46), as iron scavenging is associated with the inflammatory response (47).

Mononuclear cell infiltration was associated with sporadic localized areas of muscle necrosis in 1 macaque (Figure 2, K and L). No major abnormalities were observed in synovial samples or central nervous tissue samples of intermediate-dose animals (data not shown).

We also examined 45 tissues (including lymphoid organs, liver, muscle, joint, central nervous system, and skin) collected at 2, 5, 6, 7, and 186 dpi from 5 high-dose animals (Supplemental Table 2). No extensive mononuclear cell infiltrations were detected at 2 dpi,

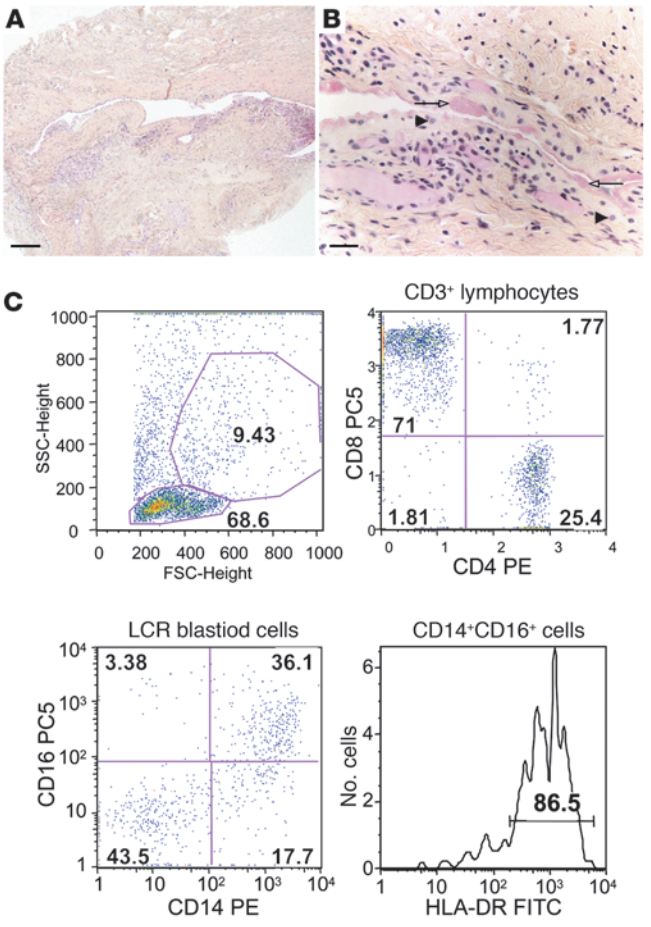

Figure 3
Mononuclear cell infiltration in tissues of macaques inoculated with high-dose CHIKV. (**A** and **B**) Tissues lesions in ankle joint collected from a 7-dpi macaque inoculated with 10^8 PFU CHIKV. Mild fibrinous exudate (arrows) was associated with mononuclear cell infiltration of the synovial tissue (arrowheads). Hematoxylin eosin safran staining. Scale bars: 300 μm (**A**); 100 μm (**B**). (**C**) Staining of cerebrospinal fluid cells collected from a macaque inoculated with 10^8 PFU showing clinical signs of meningoencephalitis. Infiltrating cells were mainly $CD8^+$ T cells and activated monocyte/macrophages ($CD14^+CD16^+HLA\text{-}DR^+$). Numbers denote percent of population in the respective gate or quadrant.

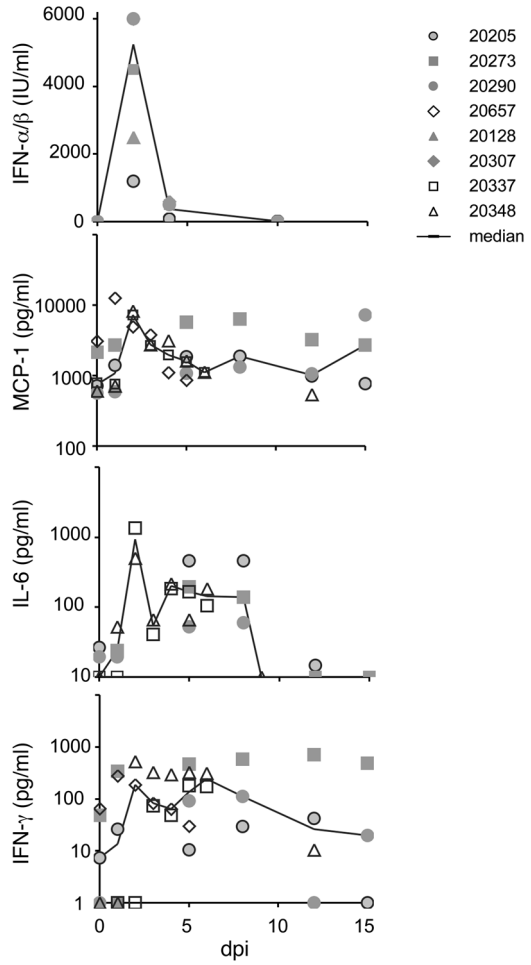

Figure 4
Kinetics of plasma inflammatory mediators. Macaques were inoculated with 10^3 PFU CHIKV. Plasma cytokines and chemokines induced by the CHIKV infection were assayed by a bioassay for IFN-α/β or using Luminex assays for CCL2 (MCP-1), IL-6, and IFN-γ.

despite a very high level of viral production in blood (7×10^7 to 5×10^9 vRNA copies/ml). As described above for macaques receiving intermediate-dose inoculates, mononuclear cell infiltrates were observed in lymphoid tissues between 5 and 186 dpi. In liver, hemosiderin accumulation was also observed. In muscle samples, moderate focal mononuclear cell infiltration was found at 186 dpi and was associated with isolated muscle fiber necrosis. Interestingly, mononuclear cell infiltration and moderate amounts of fibrinous exudates, indicative of joint inflammation, were observed in synovial tissues of 1 7-dpi animal showing swelling of joints (Figure 3, A and B). Cerebrospinal fluid (CSF) collected from a macaque showing clinical signs of meningoencephalitis revealed the presence of numerous mononuclear cells (more than 800 cells/μl) at 4 dpi. Using FACS analysis, the cells in the CSF were found to be composed predominantly of lymphocytes (67%) and monocyte/macrophages (9%). Of these, two-thirds of lymphocytes were $CD8^+$ T cells, and the monocyte/macrophages were highly activated ($CD14^+CD16^+HLA\text{-}DR^+$; Figure 3C).

In summary, these studies revealed extensive infiltration with mononuclear cells, mostly composed of macrophages, in lymphoid tissues and liver in all animals. These infiltrates appeared early in infection and in many cases persisted for at least 6 months after virus inoculation. Minor infiltration with these cells was sometimes also observed in the joints and muscles. Such monocyte/macrophage infiltrates were observed in muscle of neonates or young mice infected with CHIKV (18, 19). Similar infiltration were also reported in muscle of mice (48) or knee joints of patients after RRV infection (49), which suggests a causal relationship between monocyte/macrophage infiltration and myalgia and arthralgia/arthritis.

The cytokine pattern is consistent with monocyte recruitment and macrophage activation. Mononuclear cell infiltration appeared to be a major feature of CHIKV infection and disease. The cytokine and chemokine profiles of infected macaques were thus examined. Plasma collected from monkeys inoculated with 10^3 PFU CHIKV was analyzed using an IFN-α/β bioassay or a multiplex-microbead immunoassay. The IFN-α/β concentration increased substantially as early as 2 dpi and then fell sharply by 4 dpi, with peak IFN-α/β correlating with peak viremia (Figure 4). A rapid and large increase in CCL2 (MCP-1) levels was also observed at 1–6 dpi (Figure 4). The levels of proinflammatory cytokine IL-6 significantly increased by 2 dpi, and these high levels persisted up to 6 dpi. Finally, the level of IFN-γ increased sharply between 1 and 2 dpi and then decreased slowly over the subsequent 15 days. Comparison of cytokine levels in infected monkeys (Table 3) between baseline (before infection) and the peak of cytokine production indicated significant increases in IFN-α/β, IFN-γ, CCL2 (MCP-1), CCL3 and CCL4 (MIP-1α and MIP-1β), IL-6, and TNF-α, although the last of these showed considerable variation (Table 3).

Thus, the profile of proinflammatory mediators, which correlated with peak viremia and the decrease in $CD14^+$ cells in blood (Supplemental Table 3), was consistent with early monocyte/macrophage recruitment by MCP-1; continuous activation of macrophages by MCP-1, IFN-γ, and IFN-α/β; and secretion of IL-6 and, to a lesser extent, TNF-α by these and perhaps other cells.

CHIKV persistently infects lymphoid organs and liver and, to a lesser extent, muscle and joints. We quantified viral genomic RNA relative to endogenous control GAPDH using semiquantitative RT-PCR assays in various homogenized tissue lysates (spleen, lymph node, liver, joint, muscle, skin, brain, and spinal cord). Given that the expression of housekeeping genes may be affected by the experimental conditions (50), we first checked that GAPDH mRNA levels remained essentially unaffected in CHIKV-infected lymphoid, splenic, hepatic, and muscular tissues (Supplemental Figure 3). Relative quantification results are presented in Figure 5A. Real-time RT-PCR assays revealed high levels of CHIKV RNA in all tested tissues, particularly in lymph nodes, spleen, and liver, during the acute phase of the infection, which suggests that CHIKV efficiently disseminates into various organs. Whereas viremia peaked at 2 dpi, the viral load in most tissues reached a peak by 6 dpi and then progressively decreased in all tissues, but was still detectable in lymphoid organs until 3 months, and in liver until nearly 2 months, after inoculation. In synovial and muscular tissues, CHIKV RNA was still detected 1.5 months after inoculation. No vRNA was detected in skin or in the central nervous system beyond 1 month after inoculation, although some vRNA was present in the cerebrospinal fluid at 55 dpi. This finding demonstrated the persistence of CHIKV RNA in organs affected during human

Table 3
Cytokines and chemokines in plasma

Cytokine/ chemokine	Baseline	Acute infection	*P* vs. baseline[A]	Maximum dpi[B]
IFN-α/β	–	2,000 (1,500–25,000)	0.001	1
IFN-γ	22 ± 9	525 (217–743)	0.028	5–7
IL-2	183 ± 210	827 ± 870 (96–2,561)	0.075	9
IL-12p40	147 ± 67	252 ± 230 (177–716)	>0.1	–
IL-4	<13	<13	ND	–
IL-10	<7,12	<7,12	ND	–
IL-6	<9	503 (13–1,777)[C]	0.028	1
TNF-α	10 ± 4	48 ± 26 (16–85)	0.028	7
IL-1β	<5	<5	ND	–
IL-8 (CXCL8)	<27	<27	ND	–
MCP-1 (CCL2)	670 ± 407	47,484 (3,771–131,890)[C]	0.028	–
MIP-1α (CCL3)	51 ± 11	290 ± 267 (82–763)	0.028	7
MIP-1β (CCL4)	102 ± 28	351 ± 274 (116–836)	0.046	7
RANTES (CCL5)	2,930 ± 1,100	7,038 ± 3,084 (1,909–11,126)	0.075	–
IL-17	17 ± 4	60 (40–120)	ND	–

Cytokine and chemokine levels were followed daily for 6 animals from baseline to chronic phase, with the exception of IL-17 (2 animals tested). Values (mean ± SEM) are pg/ml with the exception of IFN-α/β (IU); ranges are given in parentheses. [A]Baseline values and maximum values during the acute phase of infection in the same monkeys were compared using Wilcoxon test; ND, not determined. [B]dpi on which the maximum value was recorded. [C]Dose response to viral input, $P < 0.04$, Fisher exact test.

disease and identified lymphoid tissue as what we believe to be a new site of viral persistence.

To further characterize the viral replication pattern in tissues showing positive quantitative RT-PCR results (i.e., spleen, muscle, and joint), 2 independent RNA in situ hybridization assays were performed using probes specific for CHIKV 26S subgenomic RNA, with a RRV 26S RNA probe used as a negative control. No signal was detected using the RRV 26S RNA probe or with the CHIK RNA probe assayed using uninfected tissues (Figure 5, C, D, F, G, I, and J). In the spleen from macaques inoculated with an intermediate 10^3-PFU CHIKV dose, strong cytoplasmic accumulations of CHIKV RNA were detected from 6 dpi in numerous mononuclear cells at the periphery of the follicular germinal center of the white pulp (Figure 5B). CHIKV genome was still detected in similarly localized cells until 55 dpi, but the intensity of staining progressively decreased with time. Some endothelial cells, localized in the splenic connective tissue trabecula, were also positive at 6 dpi (Supplemental Figure 5A). In muscles, between 6 and 55 dpi, foci of positive cells within the connective tissue surrounding muscle fibers were identified (Figure 5E). These cells had an elongated thin band of cytoplasm lining a capillary lumen and were separated from the adjacent muscle fiber by an optically empty space of 4 μm, suggestive of an endothelial cell type. Quantitative RT-PCR assays of other muscle samples at 55 dpi were below the detection limit. In 6-dpi joints, vRNA was detected in few mononuclear cells in connective tissue surrounding a zone of tendon attachment (Figure 5H). The presence of vRNA in joints at the late stage of 19 dpi was not detected by in situ hybridization. Using RT-PCR or in situ hybridization, we confirmed the persistence of CHIKV genome in spleen and muscle up to 55 dpi (Supplemental Figure 5). CHIKV RNA thus appeared to persist in splenic and synovial mononuclear cells and in muscle endothelial cells.

We next investigated the ability of CHIKV isolated from tissue lysates to replicate in mammalian or mosquito cell lines. Infected spleens, livers, muscles, and joints were minced and homogenized, and viral titers of each tissue homogenate were estimated both on BHK-21 mammalian cells by tissue culture ID_{50} ($TCID_{50}$) assays in duplicate (Figure 6) and on C6/36 mosquito cells (Supplemental Table 4). Infectious CHIKV was detected at elevated levels at 6 dpi in spleen, liver, joint (10^6 $TCID_{50}$/g), and, to a lesser extent, muscle (10^4 $TCID_{50}$/g). Infectious virus was still recovered from spleen, liver, and muscle at 44 dpi (Figure 6 and Supplemental Table 4); no significant difference in titer was found between mammalian and mosquito cell lines (data not shown). In joint, no infectious virus was found at 44 dpi, although CHIKV RNA was detected by RT-PCR at this time, probably because of differences in the sensitivity of these techniques. Interestingly, lower levels of infectious virus (<10^4 $TCID_{50}$/g) were found in livers of neonatal mice at 3, 5, and 7 dpi, whereas no virus was detected in spleen at these time points (18). In contrast, viral infectious titers in the mouse neonate model were 10 to 1,000 times greater in muscle at 5–7 dpi (18, 19). However, Ziegler et al. found that the titers in leg muscle collected from older mice were lower than those from newborn ICR or CD1 mice (19), which suggests that age may affect viral titers in these tissues. Virus isolation from tissues (Figure 6) was consistent with the results of our quantitative RT-PCR experiments showing higher levels of vRNA copies in spleen and liver than in muscle tissue (Figure 5A), with infectious CHIKV being detected in homogenates from these tissues up to 44 dpi.

Taken together, these data suggest that in immunocompetent adult nonhuman primates, CHIKV persists in lymphoid tissues, liver, joints, and muscles for up to 3 months and is able to replicate in spleen, liver, and muscle for extended periods. Furthermore, results of in situ hybridization assays suggested that the virus persists mainly in mononuclear cells and, to a lesser extent, in endothelial cells.

Macrophages, dendritic cells, and endothelial cells are infected by CHIKV, and macrophages seem to play a prominent role in persistence of the virus in macaques. Immunohistochemistry was used to detect cells positive for CHIKV antigen in tissue samples taken from macaques inoculated with intermediate or high doses of virus. There was no difference in the signal distribution or intensity between these 2 groups of macaques. CHIKV antigen was detected in the cytoplasm of numerous mononuclear cells in spleen and lymph nodes as early as 2 dpi (Table 4). Antigen-positive cells were mostly distributed around macrophage-sheathed capillaries in the splenic red pulp (Figure 7A) and in the nodal T cell areas (data not shown). There were few or no antigen-positive cells in T cell areas at 32–44 dpi, but viral antigen was found in mononuclear cells infiltrating B cell areas at 2–90 dpi (Figure 7B). Staining was clearly visible in the cytoplasm rather than exclusively on the cell surface, illustrating that this staining was not the result of Fc receptor binding (data not shown). Viral antigen was also detected in the sinusoidal endothelium of the liver (see below). The presence of viral antigen could not be unequivocally demonstrated by immunohistochemistry in skeletal muscles, synovial

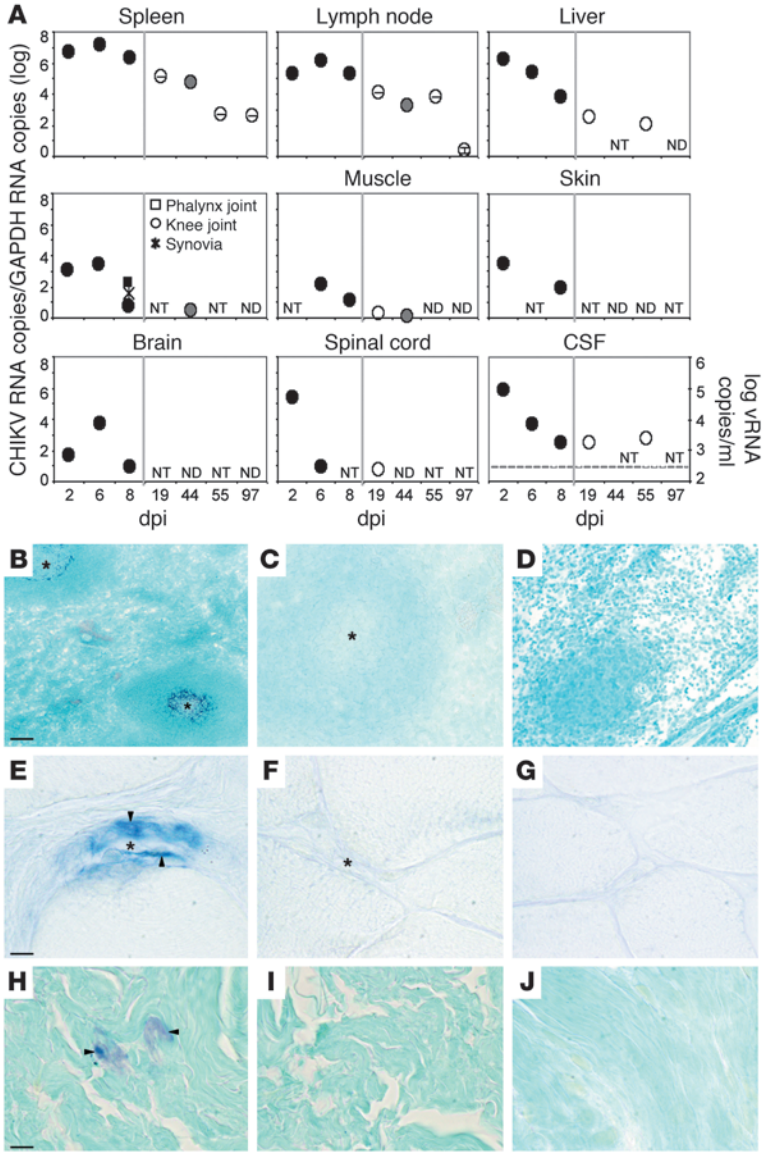

Figure 5

CHIKV distribution in organs of CHIKV-infected macaques, 2–97 dpi. (**A**) Relative quantitative RT-PCR in spleen, lymph nodes, liver, joint, and muscle of macaques inoculated with 10^3 PFU (white symbols), 10^6 PFU (gray symbols), or more than 10^7 PFU (black symbols). The CHIKV RNA copy number was normalized to GAPDH copy number. CHIKV RNA was also quantified in CSF. For each sample, the relative copy number represents the mean of at least 3 independent RT-PCR amplifications carried out on 2 independent RNA extractions. Vertical error bar denotes SEM. NT, not tested; ND, not detected. (**B**–**J**) In situ hybridization assays in spleen (**B**–**D**), muscle (**E**–**G**), and joint tissue (**H**–**J**) of macaques infected with 10^3 PFU, 6 dpi. (**B**, **E**, and **H**) CHIKV 26S RNA was detected in the cytoplasm of many mononuclear cells surrounding follicular centers (asterisks) of the splenic white pulp (**B**), and in some endothelial cells (arrowheads) surrounding vascular lumen (asterisk) of the muscular endomysial tissue (**E**). (**H**) Some vRNA was also detected in the cytoplasm of a few cells in the synovial tissue (arrowheads). (**C**, **F**, and **I**) Control assay using probe specific for RRV 26S RNA. (**D**, **G**, and **J**) Control assay using CHIKV 26S RNA on tissues of an uninfected macaque. Scale bars: 200 μm (**B**–**D**); 20 μm (**E**–**J**).

membranes, or skin connective tissues because of high background signals associated with the presence of collagen fibers.

CHIKV$^+$ tissues were further analyzed by immunofluorescence and were costained with cell type–specific markers. Viral antigen was present in CD68$^+$ macrophages from all macaques until 3 months after infection (Figure 7, D and E), with a majority of these cells in spleen being CHIKV$^+$ at 2 dpi. Other macrophage lineage cells, including hepatic Kupffer cells and neural microglia, were negative for CHIKV antigen (data not shown). CHIKV antigen was also detected early in infection in some lymphoid dendritic cells (S100$^+$; Figure 7, G and H) and in some endothelial cells (factor VIII–positive [FVIII$^+$]) of the liver sinusoids (Figure 7, J and K) and spinal cord meninges (Supplemental Figure 4, B and C). Direct examination of spleen indicated a relative amount of 1 CHIKV$^+$ dendritic cell per 10 CHIKV$^+$ macrophages. After 19 dpi, we were not able to identify CHIKV$^+$S100$^+$ cells. As described above, in situ hybridization results also suggested that positive cells in muscle connective tissue and in the splenic trabecula had the morphology of an endothelial cell type.

In order to further characterize CHIKV persistence in macrophages, combined in situ hybridization for CHIKV and immunohistochemistry for CD68 was performed in spleen of infected macaques at 6, 19, and 44 dpi. CHIKV genome was detected in macrophages at 6 dpi (Figure 8, A–C) and 19 dpi (data not shown), indicative of viral persistence rather than simply long-term retention of viral antigen in these cells. Furthermore, we confirmed that human monocyte-derived macrophages were susceptible to CHIKV LR2006-OPY1 infection in vitro (Figure 8D), as previously described for other CHIKV strains (34).

The results of the present study show, for the first time to our knowledge, that macrophages act as a cellular reservoir for the persistence of CHIKV during the late stages of infection in macaques. CHIKV persistence in macrophages may be responsible for the long-lasting symptoms observed in humans.

Discussion

Although the clinical manifestations of CHIKV infection have been well described, the pathogenesis of CHIKV disease in humans is poorly understood. Herein we provided a detailed analysis of CHIKV infection in nonhuman primates and demonstrated that experimental infection of macaques with CHIKV represents a relevant model of human CHIKV infection. We also identified macrophages as central players in CHIKV infection and persistence.

Using a virus from the recent Reunion Island outbreak, we demonstrated that CHIKV infection in macaques recapitulated the clinical and biological features observed in humans during the Reunion Island epidemic. The acute phase of infection, coinciding with peak viremia, was characterized in macaques — as it is in humans — by (a) fever and cutaneous manifestations; (b) increased levels of serum AST and ALT; (c) sharp rise, then fall, of IFN-α/β and IL-6 concentrations; (d) rapid increase, then gradual decline, of MCP-1 and IFN-γ

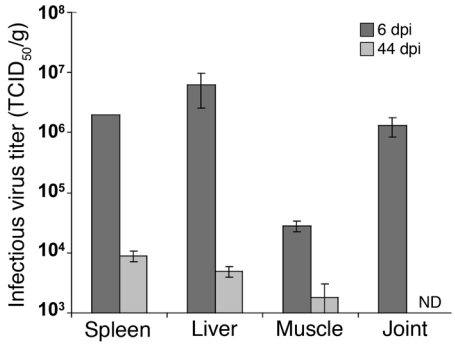

Figure 6
Infectious virus titers in spleen, liver, muscle, and joint collected from CHIKV-infected macaques, 6 and 44 dpi. Tissues were collected at 6 dpi from macaques inoculated i.v. with 10^7 PFU CHIKV, or at 44 dpi from macaques inoculated i.v. with 10^6 PFU CHIKV, and the amount of infectious virus present in tissues was quantified by $TCID_{50}$. Data are mean ± SEM of 2 independent virus titrations. The detection threshold was 700 $TCID_{50}$/g.

secretion; and (e) lymphopenia, monocytopenia, and granulocytosis, probably due in part to the presence of IFN-α and MCP-1 (51, 52). During this phase, high levels of CHIKV RNA were detected in the spleen, lymph nodes, and liver, and to a lesser extent in joints, muscle, skin, and the central nervous system. Many of these tissues are affected during human disease (12, 13). The subacute phase, beginning at the end of viremia, was characterized by (a) normalization of leukocyte counts by 10–20 dpi; (b) pronounced macrophage infiltrates in secondary lymphoid organs from 6 dpi onward; and (c) presence of vRNA and/or antigens in lymphoid organs, liver, meninges, joint, and muscle. Finally, the chronic phase was characterized by the persistence of (a) activated macrophages, (b) vRNA, and (c) antigen for up to 2 months in lymphoid organs and liver, potentially explaining the long-lasting symptoms observed in humans.

Our study also demonstrated a relationship among the amount of inoculated virus, viremia, and disease. Interestingly, we did not observe any differences between i.d. and i.v. inoculation in our model. At high doses of virus, we observed arthritis, meningoencephalitis, and death; at intermediate doses, only fever and rash were observed; and at the lowest dose, no clinical signs were observed. This spectrum of symptoms is also observed in humans. Thus, whether an infected individual develops the disease or remains asymptomatic may be determined, at least in part, by the amount of virus delivered by the mosquito. The observation that CHIKV infection in macaques mimicked CHIKV infection in humans suggests that our macaque model is a relevant model to study CHIKV disease. Mouse models of CHIKV disease have been reported, but thus far have used neonatal or young mice (18, 19) or adult mice with a totally or partially abrogated type I IFN signaling pathway (18). This contrasts with CHIKV disease in humans, which is usually milder in children (12, 40) and not restricted to immunosuppressed individuals. Furthermore, we observed that animals inoculated with the highest doses of virus produced larger amounts of IFN-α/β (about 25,000 IU/ml plasma), which did not prevent the development of viremia or disease.

A limitation of our study is the limited pathology observed in muscles or joints of macaques inoculated with the intermediate 10^3-PFU dose of viral inocula, considering these are major sites of pain in human CHIKV disease. However, the coincidence of localized pain or clinical symptoms with tissue lesions has only been demonstrated in very severe human cases (18, 33, 37, 53, 54). Similarly, in our model, only macaques infected with high doses of virus showed such a marked pathology: joint effusion, meningoencephalitis (Figure 3), and severe rash. However, we found significant macrophage infiltration and detected virus in these tissues by immunochemistry and PCR.

In order to further characterize CHIKV pathogenesis, we investigated the viral distribution and persistence in our macaque model. At early stages of infection, CHIKV was found in skeletal muscles, joints, meninges, and skin, as described in mouse models using larger viral inocula (18, 19). Interestingly, in our macaque model, CHIKV also exhibited a marked tropism for spleen, lymph nodes, and liver during the viremia peak. We believe the high level of infection of lymphoid organs is a novel finding for arthrogenic alphavirus infections, although moderate levels of spleen infection were previously reported in young and IFN-α/β receptor–deficient mice (18, 55) and in Venezuelan equine encephalitis virus infections (56). The present study also provided evidence that CHIKV can persist and replicate in vivo in primates for extended periods, with vRNA and antigen detected in several organs and tissues for 3 months. Alphaviral persistence has been described in vitro, in human synovial fibroblasts and murine macrophages (57, 58), and in vivo, in mouse muscle cells (59), up to 25 dpi with another arthrogenic alphavirus, RRV. The only study addressing in vivo persistence of alphavirus in humans found viral RNA 5 weeks after the onset of symptoms in 2 RRV disease patients (49). These findings suggest that arthrogenic alphaviruses can persist in primates for extended periods, despite the presence of antiviral antibodies and T cell responses. Such persistence may provide a possible explanation for the long-lasting symptoms observed in humans.

Our results provide compelling evidence for an important role for macrophages in the pathology of CHIKV disease. The high levels of macrophage/mononuclear cell infiltration in lymphoid organs and the large amounts of CHIKV antigen and vRNA detected in macrophages in spleen for prolonged periods (up to 3 months)

Table 4
Detection of CHIKV antigen in tissues after CHIKV infection

Organ	Localization	dpi						
		2	6	19	32	44	90	186
Spleen	Red pulp	+	+	+	+	−	+	−
Spleen	T cell area	+	+	−	−	−	−	−
Spleen	B cell area	−	−	−	+	+	+	−
Lymph node	T cell area	+	+	+	NT	−	+	−
Lymph node	B cell area	−	−	−	NT	+	+	−
Liver	Sinusoidal endothelium	+	+	+	+	+	+	−

All animals were inoculated with an intermediate dose, except the 2- and 186-dpi groups, which received high-dose CHIKV. Symbols denote detection of viral antigen or lack thereof; NT, not tested. $n = 1$ (2, 6, 44, and 186 dpi) or $n = 2$ (19, 32, and 90 dpi).

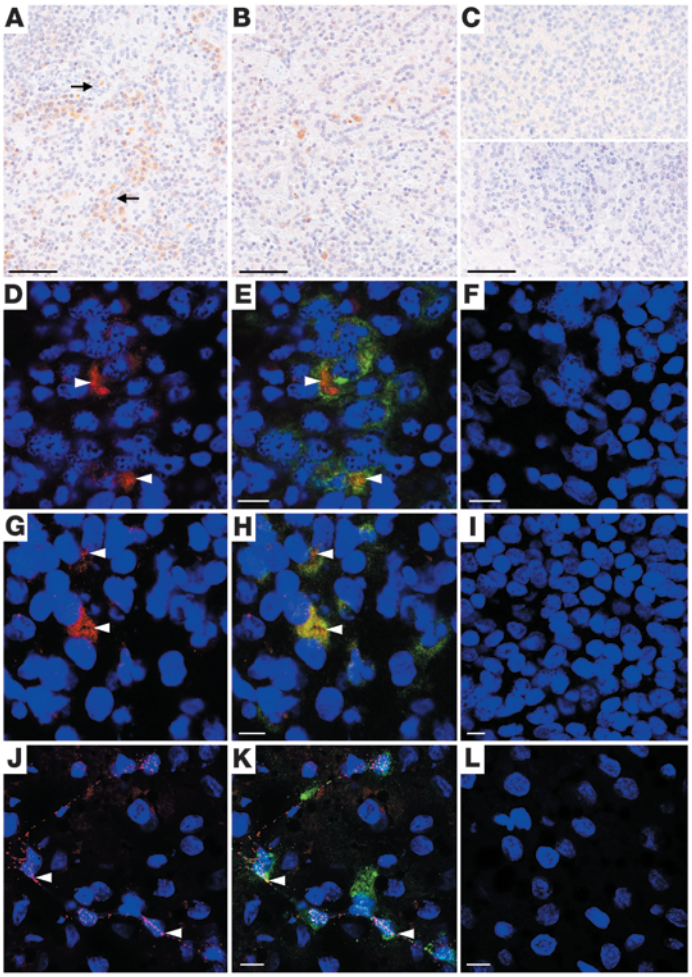

Figure 7
Immunohistochemical findings in spleen (**A**–**I**) and liver (**J**–**L**) collected from CHIKV-infected macaques at various times. (**A**) Viral antigens were detected by immunohistochemistry at 6 dpi in the cytoplasm of numerous mononuclear cells (brown staining) of the splenic red pulp. Staining was associated with pronounced macrophage infiltration (see Figure 4). Macrophage sheathed capillaries of the red pulp are denoted by arrows. (**B**) Viral antigen detected in mononuclear cells of the enlarged follicles of the splenic white pulp at 44 dpi. (**C**) Isotypic control assay (top) and control assay using splenic tissue of an uninfected macaque (bottom). (**D**–**L**) CHIKV antigen-positive cells are indicated (arrowhead). (**D** and **E**) CHIKV antigen in $CD68^+$ macrophages of the spleen, 44 dpi. (**G** and **H**) CHIKV antigen in $S100^+$ splenic dendritic cells, 6 dpi. (**J** and **K**) CHIKV antigen in $FVIII^+$ endothelial cells lining the sinusoids of the liver, 44 dpi. (**D**, **G**, and **J**) CHIKV antigen labeling is shown in red; nuclei are stained in blue. (**E**, **H**, **K**) Merged images, with cell-specific markers in green. (**F**, **I**, and **L**) Isotype control assays. Scale bars: 200 μm (**A**–**C**); 20 μm (**D**–**L**).

demonstrated that macrophages act as the cellular reservoirs for CHIKV persistence. Moreover, long-term detection of both viral genome and infectious virus in lymphoid organs, liver, and muscle was consistent with macrophages being a major site of viral replication. Although previous immunohistochemistry studies on muscles, joints, and skin in mouse models suggested that fibroblasts are the predominant target cell of CHIKV infection, CHIKV antigens were also found in a few mature macrophages in liver, spleen, and muscle of infected adult IFN-α/β receptor–deficient mice at 3 dpi (18). Our in vitro studies showed that human monocyte-derived macrophages were susceptible to CHIKV infection (Figure 8D), in agreement with previous studies in human monocyte-derived macrophages (34) and primary liver macrophages isolated from mice (18). Jaffar-Bandjee et al. also described CHIKV-infected macrophages in synovial tissue 18 months after CHIKV infection in a single patient from Reunion Island (54). Previous in vitro studies and mouse models of RRV disease have also suggested a central role for macrophages in alphaviral arthropathies (49, 60). Taken together, these results pointed to macrophages as having an important role in CHIKV infection and disease.

Cells other than monocytes/macrophages may also be involved in CHIKV pathology. Despite their relatively low number, we showed that dendritic cells were infected by CHIKV. Although we could not demonstrate CHIKV replication in dendritic cells in vivo, the high levels and diffuse distribution of CHIKV antigens in the cytoplasm of these cells were highly suggestive of productive infection. However, we and others have not been able to infect human monocyte-derived dendritic cells in vitro (Figure 8D), regardless of whether the CHIKV was derived from mammalian or mosquito cells (34). Given that dendritic cells are phenotypically heterogeneous, the exact type of dendritic cells infected in vivo remains to be determined. That alphaviruses can infect dendritic cells has been reported for RRV, Sindbis, and Venezuelan equine encephalitis viruses (61–63).

In addition to macrophages and dendritic cells, CHIKV antigen was found in endothelial cells of spinal meninges at 6 dpi, of muscle up to 55 dpi, and of liver up to 3 months after inoculation. CHIKV antigen detection in sinusoidal capillary endothelial cells has been described during the early stages of infection in IFN-α/β receptor–deficient mice (18). Infection of endothelial cells in muscle contrasts with earlier studies reporting CHIKV infection of muscular satellite cells. However, satellite cell infection was described in cases of severe and extended muscle necrosis observed in some rare patients with myositic syndrome (33) or in infected neonatal mice (18). In our model, and probably in most human cases, muscular lesions comprise only small areas of muscular infiltration by mononuclear cells and infection appears to be limited to endothelial cells.

Our present study demonstrated the importance of macrophages in primates, both as sites of infection and viral persistence and as key players in pathogenesis. One might speculate that early infection in several organs leads to recruitment of monocytes/macrophages. Viral induction of MCP-1 and IFN-α/β may be responsible for monocyte/macrophage recruitment and activation, with further activation by NK and/or T cell–derived IFN-γ also probable (60). Clinical manifestations may result from excessively activated macrophages releasing proinflammatory mediators such as IL-6 and, to a lesser extent, TNF-α (64). These observations also suggest that the chronic course of CHIKV disease in humans is caused by continuing inflammatory responses associated with persistent virus, rather than by virally induced autoimmunity (65).

In conclusion, our results provide insights into the pathogenesis of CHIKV. We have developed a relevant macaque model of CHIKV infection, in which we demonstrated long-term CHIKV persistence

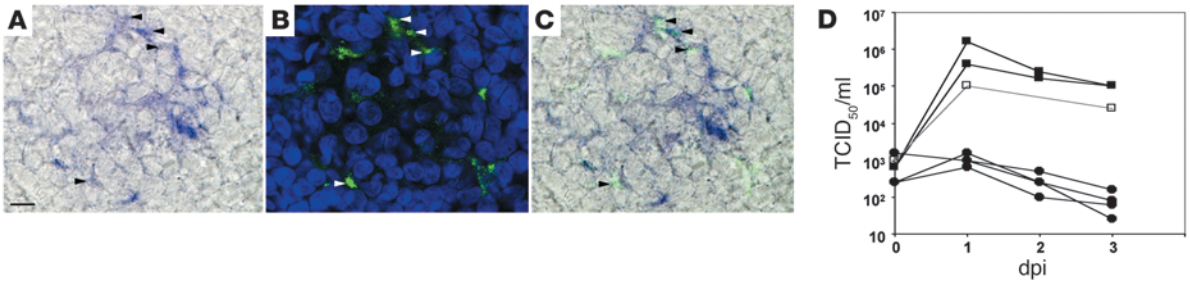

Figure 8
CHIKV infects macrophages. (**A**) Coupled in situ hybridization for CHIKV and immunohistochemistry for CD68 in spleen of macaque infected with 10^3 PFU, 6 dpi. Most mononuclear cells in which CHIKV 26S RNA was detected (**A**, arrowheads) were identified as macrophages, as they stained positive for CD68 (**B**). (**C**) Merged image. Scale bar: 20 μm. (**D**) Macrophages (squares) or dendritic cells (circles) were infected with the CHIKV LR2006-OPY1 at MOI 10 (black symbols) or MOI 5 (white symbols). Viral production was expressed as virus titers in $TCID_{50}$/ml on BHK-21 cells.

in various tissues and identified macrophages as cellular reservoirs during the late stages of CHIKV infection in vivo. The persistence of CHIKV over extended periods could explain the long-lasting symptoms, in particular arthralgia, observed in humans. A better understanding of CHIKV pathophysiology should help in the development of new therapeutic or prophylactic strategies against CHIKV disease, and this primate model also provides a system in which any new interventions can be tested.

Methods

Animals. Captive-bred 3- to 5- year-old cynomolgus macaques (*Macaca fascicularis*) were imported from Mauritius. All animals were negative for SIV, simian T lymphotropic virus, herpes B virus, filovirus, SRV-1, SRV-2, measles, dengue, and CHIKV and were maintained in a biosafety level 3 facility. Studies were approved by the regional animal care and use committee ("Comite Regional d'Ethique sur l'experimentation animale Ile de France Sud," Fontenay-aux-Roses, France) in accordance with European directive 86/609/EEC. At the end of each study, sedated animals were killed by i.v. injection of a lethal dose of pentobarbital.

Viral stock. The CHIKV strain LR2006-OPY1, a primary isolate from the recent outbreak in Reunion Island (35), was used. This strain was originally isolated from the serum of a febrile French patient returning from Reunion Island. The strain was passaged 3 times in Vero cell culture. Stock virus was produced following a single passage in BHK-21 cell culture. The in vitro titer was estimated to be 10^8 cell culture ID_{50}/ml in BHK-21 cells or 1.8×10^8 PFU/ml in Vero cells and $1.8 \pm 0.9 \times 10^{10}$ equivalent vRNA molecules/ml using the RT-PCR procedure described below.

Animal infection and bleeding. Before handling, the animals were sedated with ketamine chlorhydrate (10 mg/kg; Rhone-Mérieux). Clinical examinations were carried out, and temperature and weight recorded 15 minutes after sedation. Macaques were inoculated, either via the saphenous vein, with virus stock diluted in 1 ml phosphate-buffered saline, or via the i.d. route (10 μl diluted viral stock).

Plasma viral RNA extraction and quantification. Viral RNA was prepared from 100 μl EDTA anticoagulated, cell-free plasma, using the Nucleospin 96 Virus Kit (Macherey Nagel) according to manufacturer's instructions. RNA was eluted in 100 μl nuclease-free water and was stored at –80°C until analysis. CHIKV, diluted in an EDTA-plasma sample from CHIKV-uninfected macaques was used to generate a standard curve by serial 10-fold dilutions. 3 aliquots of the CHIKV stock and 2 EDTA-plasma samples from CHIKV-negative macaques were used as positive and negative RT-PCR controls, respectively. Standards, controls, and viral RNA samples were extracted and tested in parallel and under the same conditions. Extracted RNA (10 μl) was subjected to RT using the Superscript One-Step RT-PCR kit (Invitrogen) according to the manufacturer's recommendations, with primers ChikF1 and ChikR1 (200 nM) and the probe ChikProb (100 nM), designed by Laurent et al. (38), in a total 25 μl reaction volume. Quantitative RT-PCR was performed in an iCycler real-time thermocycler (Bio-Rad), with the following cycling conditions: 30 minutes at 56°C, then 5 minutes at 95°C, followed by 50 cycles at 95°C for 15 seconds and 60°C for 1 minute. All amplifications were performed in duplicate. The standard RNA template dilution showed a correlation coefficient of 98%–99% over 7 orders of magnitude, with a sensitivity corresponding to 10^3 RNA copies/ml or 20 copies per sample.

Tissue viral RNA extraction, quantification, and analysis. Tissue lysates were obtained by mechanical disruption of tissue samples in lysis buffer (Macherey Nagel) with a Precellys system, using tubes with ceramic beads (Bertin technologies). The tissue lysate was then diluted to 30 mg/ml in Macherey-Nagel lysis buffer, aliquoted, and stored at –80°C until extraction. Total RNA was extracted in duplicate from lysate aliquots using the Nucleospin 96 RNA kit (Macherey Nagel), following the manufacturer's instructions. Relative quantitative RT-PCR was carried out, as described above, simultaneously with CHIKV and GAPDH primers and probes (sequences described in refs. 38 and 66, respectively). RT-PCR assay efficiencies were determined using standard dilution curves (10-fold serial dilution) for CHIKV and GAPDH series. As all the reactions were approximately 100% efficient, each CHIKV sample was normalized using a duplicate GAPDH sample, and the relative copy number for each sample was calculated as follows: $2^{-(Ct\ CHIKV - Ct\ GAPDH)}$. For each sample, the relative copy number was the mean of at least 3 independent RT-PCRs using 2 independent RNA extractions. Finally, averages were normalized for each tissue relative to the detection threshold.

Cytokine and chemokine measurements. The concentrations of cytokines/chemokines in monkey plasma was determined by Luminex technology using antibodies crossreactive with cynomolgus macaque cytokines as described previously (67) and according to the manufacturer's instructions. MCP-1 and IFN-γ were assayed using Biosource (Cliniscience SA), and IL-6 was measured using Upstate (Millipore) beads and antibody pairs. IFN-α/β was measured by bioassay as described previously (68).

Histology and immunohistochemistry. We sampled 45 different tissues in duplicate during complete necropsy examination of each of 18 macaques. Either tissues were frozen and 8-μm-thick sections were cut, or tissues were fixed in 10% neutral buffered formalin, embedded in paraffin wax, and 6-μm-thick sections were cut and stained with hematoxylin eosin safranin. During morphological analysis, macrophages were identified by their abundant eosinophilic cytoplasm, euchromatic nucleus, and promi-

nent nucleolus. Liver sections were also stained with Fouchet for bilirubin and Perls for hemosiderin.

Immunohistochemical analysis involved the use of immunoperoxidase techniques for paraffin-embedded sections and indirect immunofluorescence for frozen sections. Hyperimmune mouse ascitic fluid (69) and monoclonal antibody 3E4 (70), provided by P. Desprès (Pasteur Institute), were used as primary antibodies (at dilutions of 1:1,600 and 1:200, respectively). Other antibodies used were anti-CD68 (clone KP1) for macrophages (Abcam), anti-S100 for dendritic cells, and anti–FVIII-related antigen for endothelial cells (Dako).

Paraffin-embedded sections were pretreated at 98°C for 40 minutes in citrate buffer (Dako) then incubated in 3% hydrogen peroxide for 10 minutes and in 20% normal goat serum (Dako) and 0.2% Tween (Sigma-Aldrich) for 30 minutes. They were then incubated with primary antibody in 2% goat serum, 2% BSA (Sigma-Aldrich), and 0.2% Tween overnight at 4°C and with biotinylated secondary antibodies (E433; Dako) in 20% normal goat serum and 0.2% Tween for 30 minutes; bound antibodies were detected either with streptavidin (P397; Dako) and DAB Liquid Substrate (Dako) for immunoperoxidase or with Alexa Fluor 555–conjugated streptavidin (Invitrogen) for immunofluorescence, following the manufacturer's instructions. Nuclei were stained with Topro-3 diluted 1:1,000 (Invitrogen), and sections were mounted using Mowiol medium (Calbiochem). Sections of tissues from an uninfected macaque were used as negative controls. Immunofluorescent labeling was assessed by serial scanning with He-Ne and argon ion lasers and C1 Nikon laser scanning confocal microscope. The autofluorescence associated with hemosiderin pigment in Kupffer cells of the liver was distinguished from the specific signal by multispectral analysis using a C1-SHS Nikon multispectral confocal microscope. The extent of apoptosis in liver sections was evaluated with an in situ cell death detection kit (Roche) according to the manufacturer's instructions. The numbers of total and apoptotic hepatocytes were calculated (variation coefficient, 3.4%) after random selection of 2 microscopic fields, such that more than 400 hepatocytic nuclei were scored for each sample (483 ± 49 per sample).

Flow cytometry. Flow cytometry was performed on either FACScan or LSR1 apparatus (BD Biosciences) using CellQuest software. Percentages of $CD4^+$ and $CD8^+$ T lymphocytes and monocytes were determined with direct immunofluorescence labeling. Cerebrospinal fluid (2 ml) collected from a monkey inoculated with 10^8 PFU was centrifuged, and cells were resuspended in 100 μl phosphate-buffered saline. Resuspended cells (50 μl) were then incubated at room temperature for 15 minutes with anti-rhesus CD3–FITC (clone sp34-2; BD Biosciences — Pharmingen), anti-human CD4–PE (L200; BD Biosciences) and CD8-PC5 (SK1; BD Biosciences) monoclonal antibodies to estimate lymphocyte infiltrate proportion. Populations of monocytes were evaluated using anti-human HLA-DR–FITC (clone G46.6; BD Biosciences — Pharmingen; or clone B8.12.2; Beckman Coulter), CD14-PE (clone M5E2; BD Biosciences — Pharmingen), and CD16-PC5 (clone 3G8; BD) by the same procedure.

In situ hybridization. Hybridizations were performed with a DIG-UTP–labeled CHIKV-specific riboprobe derived from pCRII-TOPO-CHIKV plasmid. A 450-bp conservative region of the virus genome, mainly specific to the 26S subgenomic RNA (region 7,371–7,820 on CHIKV LR2006-OPY1 strain, accession no. DQ443544), was amplified by RT-PCR, purified, and cloned into the pCRII-TOPO vector using a TOPO-TA cloning kit (Invitrogen) according to the manufacturer's instructions (71). A riboprobe specific for the RRV (complementary for RRV nucleotides 7,393–7,871), synthesized as described above, was used as a control for nonspecific binding (71–73). Presence and orientation of the CHIKV and RRV inserts into pCRII-TOPO plasmids were screened by sequencing. Antisense riboprobes were obtained as follows. Plasmids were linearized with either BamHI and NotI for the CHIKV plasmid, or KpnI and NotI for the RRV plasmid, and labeled according to the manufacturer's instructions by in vitro transcription with either T7 or SP6 polymerase, using a digoxigenin labeling kit (DIG RNA Labeling; Roche).

All steps before and during hybridization were carried out under RNase-free conditions. After drying, sections were postfixed in 4% PFA and pretreated with 0.2% DEPC in 2× sodium chloride sodium citrate buffer (SSC; 0.6 M, pH 7; Dako) at room temperature for 30 minutes. Sections were prehybridized for 60 minutes at 42°C in hybridization buffer containing 50% deioned formamide, 10% (w/v) dextran sulfate, 4× SSC, 1× Denhardt's solution, 10× blocking solution (Roche), and 425 μg/ml salmon fish DNA, then hybridized overnight at 42°C with 1 μg/ml CHIKV antisense probes diluted in hybridization buffer. Negative controls were RRV probes. Slides were then washed with 2× SSC and treated for 20 minutes at 37°C with 5 μg/ml RNaseA in NTE buffer (0.5 M NaCl, 10 mM Tris-HCl, and 1 mM EDTA, pH 8.0). After stringent washing for 30 minutes with 60% (v/v) formamide plus 0.2× SSC at 37°C, sequential washes were performed with 2× SSC (2×, each 10 minutes), buffer 1 (0.1 M Tris and 0.15 NaCl, pH 7.5) containing 5% blocking reagent (Roche) for 30 minutes, and buffer 1 containing 1% BSA and 0.3% Triton X-100 for 30 minutes. Slides were incubated for 2 hours at room temperature with alkaline phosphatase–conjugated sheep anti-DIG antibody (Roche), diluted 1:1,000 in buffer 1, and sequentially washed with buffer 1 (3×, each 5 minutes) and buffer 2 (0.1 mM Tris-HCl, 0.1 M NaCl, and 50 mM $MgCl_2$, pH 9.5) for 10 minutes. Slides were then incubated with alkaline phosphatase substrate (NBT/BCIP; Roche) for 2 hours. Finally, after washing, slides were counterstained with fast green for 5 seconds, dehydrated, and mounted.

Viral titrations in tissue samples. Splenic, hepatic, muscular, and joint tissues collected from macaques inoculated with 10^7 (6 dpi) or 10^6 (44 dpi) PFU were weighted, and tissues (approximatively 100 mg) were titrated and homogenized in DMEM supplemented with 10% FCS (1 ml) using tubes with ceramic beads and a Precellys system (Bertin technologies). Viral titers of each tissue sample were determined on mammalian BHK-21 cell lines based on their $TCID_{50}$ using 4–5 replicates. After 3 days of incubation, the plates were stained with crystal violet to visualize cytopathic effects. 2 independent virus titrations were carried out, and viral titers were expressed as $TCID_{50}$/g.

In vitro infection of macrophages and dendritic cells. Monocytes were isolated from buffy-coat PBMCs using elutriation or $CD14^+$ magnetic beads (Miltenyi Biotec) and were cultured for 6 days in DMEM with 10% FCS supplemented with either M-CSF (10 ng/ml) and GM-CSF (1 ng/ml) or GM-CSF (20 ng/ml) and IL-4 (20 ng/ml) for differentiation of macrophages or dendritic cells, respectively. By day 7, macrophages or dendritic cells were infected with the CHIKV viral stock for 3 hours and extensively washed. Supernatants were collected at the indicated time points, and viral titers were evaluated on BHK-21 cell lines using $TCID_{50}$/ml as above.

Statistics. We used nonparametric Spearman rank correlation tests as well as Wilcoxon and MWU rank tests adapted to small sample sizes and non-Gaussian distribution using StatView software (SAS Institute). A P value less than 0.05 was considered significant. Viral production during a selected period of time was measured by computation of the AUC using the Trapezoid calculation.

Acknowledgments

We acknowledge Clementine Schilte and the Center for Human Immunology (Pasteur Institute) as well as Karine Patient and the Immunoanalysis Studies and Research Laboratory (LERI; iBiTec-S, CEA) for support in conducting the Luminex studies; G. Gras and O. Bourry for helpful discussions; and P. Desprès (Pasteur Institute) for providing CHIKV antibodies. This work was supported by the CEA and the "Programme Transversal de Recherches Chi-

kungunya" from the French Health directorate. Travel between Australia and France was funded by French Australian Science and Technology (FAST) Program grant 16104ZM. The FAST Program is jointly managed by the Department of Innovation, Industry, Science and Research (Innovation) and its French counterparts, the Ministry of Higher Education and Research (MESR) and the Ministry of Foreign and European Affairs (MAEE).

Received for publication June 5, 2009, and accepted in revised form January 6, 2010.

Address correspondence to: Pierre Roques, Service d'immuno-virologie, Commissariat à l'Energie Atomique, DSV/iMETI, 18 route du Panorama, 92265, Fontenay-aux-Roses, Cedex, France. Phone: 33.1.46.54.91.67; Fax: 33.1.46.54.77.26; E-mail: pierre.roques@cea.fr.

1. Mason PJ, Haddow AJ. An epidemic of virus disease in Southern Province, Tanganyika Territory, in 1952–53; an additional note on Chikungunya virus isolations and serum antibodies. *Trans R Soc Trop Med Hyg*. 1957;51(3):238–240.
2. Brighton SW, Prozesky OW, de la Harpe AL. Chikungunya virus infection. A retrospective study of 107 cases. *S Afr Med J*. 1983;63(9):313–315.
3. McGill PE. Viral infections: alpha-viral arthropathy. *Baillieres Clin Rheumatol*. 1995;9(1):145–150.
4. Powers AM, Logue CH. Changing patterns of chikungunya virus: re-emergence of a zoonotic arbovirus. *J Gen Virol*. 2007;88(Pt 9):2363–2377.
5. Mavalankar D, Shastri P, Raman P. Chikungunya epidemic in India: a major public-health disaster. *Lancet Infect Dis*. 2007;7(5):306–307.
6. Pastorino B, et al. Epidemic resurgence of Chikungunya virus in democratic Republic of the Congo: identification of a new central African strain. *J Med Virol*. 2004;74(2):277–282.
7. Peyrefitte CN, et al. Chikungunya virus, Cameroon, 2006. *Emerg Infect Dis*. 2007;13(5):768–771.
8. Saxena SK, Singh M, Mishra N, Lakshmi V. Resurgence of chikungunya virus in India: an emerging threat. *Euro Surveill*. 2006;11(8):E060810.2.
9. Yergolkar PN, et al. Chikungunya outbreaks caused by African genotype, India. *Emerg Infect Dis*. 2006; 12(10):1580–1583.
10. Gerardin P, et al. Estimating Chikungunya prevalence in La Reunion Island outbreak by serosurveys: two methods for two critical times of the epidemic. *BMC Infect Dis*. 2008;8:99.
11. Sissoko D, et al. Seroprevalence and risk factors of chikungunya virus infection in Mayotte, Indian Ocean, 2005–2006: a population-based survey. *PLoS ONE*. 2008;3(8):e3066.
12. Renault P, et al. A major epidemic of chikungunya virus infection on Reunion Island, France, 2005–2006. *Am J Trop Med Hyg*. 2007;77(4):727–731.
13. Economopoulou A, et al. Atypical Chikungunya virus infections: clinical manifestations, mortality and risk factors for severe disease during the 2005–2006 outbreak on Reunion. *Epidemiol Infect*. 2009;137(4):534–541.
14. Dominguez M, and Economopoulou A. Active surveillance system for hospitalized atypical forms of chikungunya fever, Reunion Island, March 2005–April 2006. Saint-Maurice: Institut de Veille Sanitaire. http://www.invs.sante.fr/publications/2007/chik_surveillance_2007/. Published online August 2, 2007. Accessed January 8, 2010.
15. Borgherini G, et al. Persistent arthralgia associated with chikungunya virus: a study of 88 adult patients on Reunion Island. *Clin Infect Dis*. 2008; 47(4):469–475.
16. Queyriaux B, Simon F, Grandadam M, Michel R, Tolou H, Boutin JP. Clinical burden of Chikungunya virus infection. *Lancet Infect Dis*. 2008;8(1):2–3.
17. Simon F, et al. Chikungunya infection: an emerging rheumatism among travelers returned from Indian Ocean islands. Report of 47 cases. *Medicine (Baltimore)*. 2007;86(1):123–137.
18. Couderc T, et al. A mouse model for Chikungunya: young age and inefficient type-I interferon signaling are risk factors for severe disease. *PLoS Pathog*. 2008; 4(2):e29.
19. Ziegler SA, Lu L, da Rosa AP, Xiao SY, Tesh RB. An animal model for studying the pathogenesis of Chikungunya virus infection. *Am J Trop Med Hyg*. 2008;79(1):133–139.
20. Reed DS, Lind CM, Lackemeyer MG, Sullivan LJ, Pratt WD, Parker MD. Genetically engineered, live, attenuated vaccines protect nonhuman primates against aerosol challenge with a virulent IE strain of Venezuelan equine encephalitis virus. *Vaccine*. 2005; 23(24):3139–3147.
21. Verrier B, et al. Evaluation in rhesus macaques of Tat and rev-targeted immunization as a preventive vaccine against mucosal challenge with SHIV-BX08. *DNA Cell Biol*. 2002;21(9):653–658.
22. Vierboom MP, Jonker M, Tak PP, Hart BA. Preclinical models of arthritic disease in non-human primates. *Drug Discov Today*. 2007;12(7–8):327–335.
23. Walsh GP, et al. The Philippine cynomolgus monkey (Macaca fasicularis) provides a new nonhuman primate model of tuberculosis that resembles human disease. *Nat Med*. 1996;2(4):430–436.
24. Binn LN, Harrison VR, Randall R. Patterns of viremia and antibody observed in rhesus monkeys inoculated with chikungunya and other serologically related group A arboviruses. *Am J Trop Med Hyg*. 1967;16(6):782–785.
25. Inoue S, et al. Distribution of three arbovirus antibodies among monkeys (Macaca fascicularis) in the Philippines. *J Med Primatol*. 2003;32(2):89–94.
26. Kaschula VR, Van Dellen AF, de Vos V. Some infectious diseases of wild vervet monkeys (Cercopithecus aethiops pygerythrus) in South Africa. *J S Afr Vet Assoc*. 1978;49(3):223–227.
27. Kirya BG, Okia NO. A yellow fever epizootic in Zika Forest, Uganda, during 1972: Part 2: Monkey serology. *Trans R Soc Trop Med Hyg*. 1977;71(4):300–303.
28. Marchette NJ, Rudnick A, Garcia R, MacVean DW. Alphaviruses in Peninsular Malaysia: I. Virus isolations and animal serology. *Southeast Asian J Trop Med Public Health*. 1978;9(3):317–329.
29. McCrae AW, Henderson BE, Kirya BG, Sempala SD. Chikungunya virus in the Entebbe area of Uganda: isolations and epidemiology. *Trans R Soc Trop Med Hyg*. 1971;65(2):152–168.
30. Peiris JS, Dittus WP, Ratnayake CB. Seroepidemiology of dengue and other arboviruses in a natural population of toque macaques (Macaca sinica) at Polonnaruwa, Sri Lanka. *J Med Primatol*. 1993; 22(4):240–245.
31. Levitt NH, Ramsburg HH, Hasty SE, Repik PM, Cole FE Jr, Lupton HW. Development of an attenuated strain of chikungunya virus for use in vaccine production. *Vaccine*. 1986;4(3):157–162.
32. Paul SD, Singh KR. Experimental infection of Macaca radiata with Chikungunya virus and transmission of virus by mosquitoes. *Indian J Med Res*. 1968;56(6):802–811.
33. Ozden S, et al. Human muscle satellite cells as targets of chikungunya virus infection. *PLoS ONE*. 2007; 2(6):e527.
34. Sourisseau M, et al. Characterization of reemerging chikungunya virus. *PLoS Pathog*. 2007;3(6):e89.
35. Parola P, et al. Novel chikungunya virus variant in travelers returning from Indian Ocean islands. *Emerg Infect Dis*. 2006;12(10):1493–1499.
36. Vazeille M, et al. Two chikungunya isolates from the outbreak of La Reunion (Indian Ocean) exhibit different patterns of infection in the mosquito, Aedes albopictus. *PLoS ONE*. 2007;2(11):e1168.
37. Gerardin P, et al. Multidisciplinary prospective study of mother-to-child chikungunya virus infections on the island of La Reunion. *PLoS Med*. 2008; 5(3):e60.
38. Laurent P, et al. Development of a sensitive real-time reverse transcriptase PCR assay with an internal control to detect and quantify chikungunya virus. *Clin Chem*. 2007;53(8):1408–1414.
39. Panning M, Grywna K, van Esbroeck M, Emmerich P, Drosten C. Chikungunya Fever in travelers returning to europe from the Indian ocean region, 2006. *Emerg Infect Dis*. 2008;14(3):416–422.
40. Borgherini G, et al. Outbreak of chikungunya on Reunion Island: early clinical and laboratory features in 157 adult patients. *Clin Infect Dis*. 2007; 44(11):1401–1407.
41. Pialoux G, Gauzere BA, Jaureguiberry S, Strobel M. Chikungunya, an epidemic arbovirosis. *Lancet Infect Dis*. 2007;7(5):319–327.
42. Ng LF, et al. IL-1beta, IL-6, and RANTES as biomarkers of Chikungunya severity. *PLoS ONE*. 2009; 4(1):e4261.
43. Tournebize P, Charlin C, Lagrange M. Neurological manifestations in Chikungunya: about 23 cases collected in Reunion Island [In French]. *Rev Neurol (Paris)*. 2009;165(1):48–51.
44. Krakowka S, et al. Features of cell degeneration and death in hepatic failure and systemic lymphoid depletion characteristic of porcine circovirus-2-associated postweaning multisystemic wasting disease. *Vet Pathol*. 2004;41(5):471–481.
45. Ellis AE, et al. Pathology and epidemiology of natural West Nile viral infection of raptors in Georgia. *J Wildl Dis*. 2007;43(2):214–223.
46. Kage M, et al. Pathology of chronic hepatitis C in children. Child Liver Study Group of Japan. *Hepatology*. 1997;26(3):771–775.
47. Kobune M, Kohgo Y, Kato J, Miyazaki E, Niitsu Y. Interleukin-6 enhances hepatic transferrin uptake and ferritin expression in rats. *Hepatology*. 1994; 19(6):1468–1475.
48. Lidbury BA, Simeonovic C, Maxwell GE, Marshall ID, Hapel AJ. Macrophage-induced muscle pathology results in morbidity and mortality for Ross River virus-infected mice. *J Infect Dis*. 2000;181(1):27–34.
49. Soden M, et al. Detection of viral ribonucleic acid and histologic analysis of inflamed synovium in Ross River virus infection. *Arthritis Rheum*. 2000; 43(2):365–369.
50. Mogal A, Abdulkadir SA. Effects of histone deacetylase inhibitor (HDACi); trichostatin-A (TSA) on the expression of housekeeping genes. *Mol Cell Probes*. 2006;20(2):81–86.
51. Corssmit EP, et al. Effects of interferon-alpha (IFN-alpha) administration on leucocytes in healthy humans. *Clin Exp Immunol*. 1997;107(2):359–363.
52. Tsou CL, et al. Critical roles for CCR2 and MCP-3 in monocyte mobilization from bone marrow and recruitment to inflammatory sites. *J Clin Invest*. 2007;117(4):902–909.
53. Jaffar-Bandjee MC, et al. Identification des cellules cibles et des mécanismes physiopathologiques du virus Chikungunya. In: *Chikungunya et autres arboviroses émergentes en milieu tropical*. Saint-Pierre, La Réunion; 2007. URL: http://www.invs.sante.fr/agenda/colloque_chikungunya/programme_chik_version_longue.pdf. Poster 111. Accessed 2 March 2009.
54. Jaffar-Bandjee MC, et al. Chikungunya virus takes

centre stage in virally induced arthritis: possible cellular and molecular mechanisms to pathogenesis. *Microbes Infect*. 2009;11(14–15):1206–1208.
55. Ryman KD, Klimstra WB, Nguyen KB, Biron CA, Johnston RE. Alpha/beta interferon protects adult mice from fatal Sindbis virus infection and is an important determinant of cell and tissue tropism. *J Virol*. 2000;74(7):3366–3378.
56. Paessler S, et al. Inhibition of alphavirus infection in cell culture and in mice with antisense morpholino oligomers. *Virology*. 2008;376(2):357–370.
57. Journeaux SF, Brown WG, Aaskov JG. Prolonged infection of human synovial cells with Ross River virus. *J Gen Virol*. 1987;68(Pt 12):3165–3169.
58. Way SJ, Lidbury BA, Banyer JL. Persistent Ross River virus infection of murine macrophages: an in vitro model for the study of viral relapse and immune modulation during long-term infection. *Virology*. 2002;301(2):281–292.
59. Murphy FA, Taylor WP, Mims CA, Marshall ID. Pathogenesis of Ross River virus infection in mice. II. Muscle, heart, and brown fat lesions. *J Infect Dis*. 1973;127(2):129–138.
60. Suhrbier A, La Linn M. Clinical and pathologic aspects of arthritis due to Ross River virus and other alphaviruses. *Curr Opin Rheumatol*. 2004;16(4):374–379.
61. Gardner JP, et al. Infection of human dendritic cells by a sindbis virus replicon vector is determined by a single amino acid substitution in the E2 glycoprotein. *J Virol*. 2000;74(24):11849–11857.
62. Nishimoto KP, et al. Restricted and selective tropism of a Venezuelan equine encephalitis virus-derived replicon vector for human dendritic cells. *Viral Immunol*. 2007;20(1):88–104.
63. Shabman RS, et al. Differential induction of type I interferon responses in myeloid dendritic cells by mosquito and mammalian-cell-derived alphaviruses. *J Virol*. 2007;81(1):237–247.
64. Ackermann C, Kavanaugh A. Tumor necrosis factor as a therapeutic target of rheumatologic disease. *Expert Opin Ther Targets*. 2007;11(11):1369–1384.
65. Suhrbier A, Mahalingam S. The immunobiology of viral arthritides. *Pharmacol Ther*. 2009; 124(3):301–308.
66. Hu LH, Chen FH, Li YR, Wang L. Real-time determination of human telomerase reverse transcriptase mRNA in gastric cancer. *World J Gastroenterol*. 2004; 10(23):3514–3517.
67. Giavedoni LD. Simultaneous detection of multiple cytokines and chemokines from nonhuman primates using luminex technology. *J Immunol Methods*. 2005;301(1–2):89–101.
68. Malleret B, et al. Primary infection with simian immunodeficiency virus: plasmacytoid dendritic cell homing to lymph nodes, type I interferon, and immune suppression. *Blood*. 2008;112(12):4598–4608.
69. Schuffenecker I, et al. Genome microevolution of chikungunya viruses causing the Indian Ocean outbreak. *PLoS Med*. 2006;3(7):e263.
70. Brehin AC, et al. Production and characterization of mouse monoclonal antibodies reactive to Chikungunya envelope E2 glycoprotein. *Virology*. 2008; 371(1):185–195.
71. Heise MT, et al. An attenuating mutation in nsP1 of the Sindbis-group virus S.A.AR86 accelerates nonstructural protein processing and up-regulates viral 26S RNA synthesis. *J Virol*. 2003;77(2):1149–1156.
72. Heise MT, Simpson DA, Johnston RE. Sindbis-group alphavirus replication in periosteum and endosteum of long bones in adult mice. *J Virol*. 2000;74(19):9294–9299.
73. Morrison TE, et al. Characterization of Ross River virus tropism and virus-induced inflammation in a mouse model of viral arthritis and myositis. *J Virol*. 2006; 80(2):737–749.